LANGMUIR

Article

pubs.acs.org/Langmuir

Self-Diffusiophoresis of Janus Catalytic Micromotors in Confined Geometries

Fengchang Yang,[†] Shizhi Qian,[‡] Yiping Zhao,[§] and Rui Qiao*[,†]

[†]Department of Mechanical Engineering, Virginia Polytechnic Institute and State University, 460 Old Turner Street, Blacksburg, Virginia 24061, United States

[‡]Department of Mechanical & Aerospace Engineering, Old Dominion University, 5115 Hampton Boulevard, Norfolk, Virginia 23529, United States

[§]Department of Physics and Astronomy, The University of Georgia, Athens, Georgia 30602, United States

Supporting Information

ABSTRACT: The self-diffusiophoresis of Janus catalytic micromotors (JCMs) in confined environment is studied using direct numerical simulations. The simulations revealed that, on average, the translocation of a JCM through a short pore is moderately slowed down by the confinement. This slowdown is far weaker compared to the transport of particles through similar pores driven by forces induced by external means or passive diffusiophoresis. Pairing of two JCMs facilitates the translocation of the one JCM entering the pore first but slows down the second JCM. Depending on its initial orientation, a JCM near the entrance of a pore can exhibit different rotational motion, which determines whether it can enter the pore. Once a JCM enters a narrow pore, it can execute a self-alignment process after which it becomes fully aligned with the pore axis and moves to the center line of the pore. Analysis of these results showed that, in addition to hydrodynamic effect, the translation and rotation of JCM is also affected by the "chemical effects", i.e., the modification of the chemical species concentration around a JCM by confining walls and neighboring JCMs. These chemical effects are unique to the self-diffusiophoresis of JCMs and should be considered in design and operations of JCMs in confined environment.

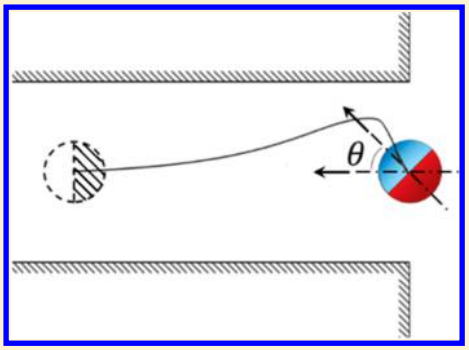

1. INTRODUCTION

Janus catalytic micromotors (JCMs) are micro/nanoscale particles that feature heterogeneous catalytic coating on their surfaces. By using the catalytic reactions on their surfaces to break down the reactants in surrounding fluids, JCMs can "swim" autonomously via various mechanisms. Since achieving autonomous movement of small particulates has long been sought in diverse fields including biology and medicine, the demonstration of autonomous JCMs about a decade ago[1,2] has triggered intensive studies of JCMs and their dynamics since then.[3,4] While the practical application of JCMs remains limited at present, autonomous JCMs have already been used successfully to sense, detect, and deliver micro/nanoparticles of various sizes and shape.[5−7] With further development, JCMs can conceivably be used to execute more demanding tasks such as removing blood clots in capillaries and environment remediation.[8,9]

The intensive experimental and theoretical studies on JCMs have tremendously improved the fabrication, operation, and understanding of JCMs. Several mechanisms including self-diffusiophoresis,[10,11] self-electrophoresis,[12] and bubble propulsion[13−15] have been revealed to drive JCMs' movement. Of these mechanisms, self-diffusiophoresis and self-electrophoresis-driven dynamics of JCMs have received the most attention. The effects of JCM design,[16,17] operating conditions such as solution composition,[18,19] geometrical confinement,[20,21] and externally imposed shear flows on the dynamics of JCM have been explored in great detail.[22] For the applications of JCMs in drug delivery and microfluidics, the geometrical confinement usually plays an important role in the JCM dynamics. Because of the importance of boundaries, several studies recently have sought to understand the role of solid boundaries in determining the JCM motion. Specifically, the self-diffusiophoresis of an active particle in the vicinity of a planar boundary has been explored via either experimental or theoretical methods.[23−27] For example, Uspal et al. investigated the self-propulsion of a catalytic active particle near a wall by combining analytical analysis and numerical simulations.[23] It was discovered that, depending on the choice of design parameters (catalytic coverage, surface mobility, etc.), the catalytic active particle shows different behaviors near a wall including reflection, steady sliding, and hovering. They suggested that the hydrodynamic effect of the wall is mainly responsible for the behaviors of catalytic active particles. Ibrahim et al. captured the wall-induced distortion of solute concentration gradients, which caused wall-induced-diffusiophoresis of JCMs.[24] Such wall-induced-diffusiophoresis promotes the translation of JCMs without affecting their rotation. Some of the simulation

Received: March 29, 2016
Revised: May 16, 2016
Published: May 17, 2016

DOI: 10.1021/acs.langmuir.6b01214
Langmuir 2016, 32, 5580−5592

predictions have been observed experimentally; e.g., Kreuter et al. observed sliding and reflection of JCM near channel walls.[25] In one recent experimental study, boundaries are used to steer the motion of JCMs and eliminate the Brownian rotation of JCM.[27] A key concept emerging from these studies is that, in addition to the hydrodynamic interactions, "chemical" interactions can also greatly affect the dynamics of JCMs under wall confinements. Specifically, the confining walls affect the transport of reaction product and cause the product concentration field near the JCM (and consequently the slip velocity and the viscous stress on the JCM's surface) to deviate from those in bulk solutions. These "chemical" interactions also affect the dynamics of a cluster of particles when they approach each other.[16,28,29]

While previous research on JCMs has greatly improved our understanding of their dynamics in free solutions and near planar boundaries,[11,23,30,31] the dynamics of JCMs in more complex environments remain to be clarified. For drug delivery and microfluidic applications, JCMs often must operate under confined conditions; e.g., multiple JCMs may come close to each other and translate through a short micropore. How the dynamics of JCM is changed by the severe confinement is not well understood. For example, how do JCMs translate through a micropore? Can a JCM enter a pore if it is not perfectly aligned with the pore axis? How do JCMs disturbed by external stimulus or thermal fluctuation behave inside a pore? There exist a few studies on these questions and useful insights were reported; e.g., the dynamics of catalytic dimer in a channel has been studied using simulations, and the effect of confinement on the reaction product concentration was shown to affect the dimer transport.[21] However, in general, research on these questions is rather scarce at present. Furthermore, most existing studies of JCM dynamics are based on quasi-static models. In these models, the reaction product concentration field is assumed to have no memory, which may not hold for highly confined JCMs.

In this work, we solve the fully coupled fluid−structure interaction problem of JCM locomotion in confined geometries using the arbitrary Lagrangian−Eulerian (ALE) method. This method allows us to remove the restriction of assuming quasi-static reaction product concentration field when solving JCM dynamics. The rest of paper is organized as follows: In section 2, we introduce the mathematical model of self-diffusiophoresis of JCM and its numerical implementation. In section 3, we systematically investigate how confinement affects the translation of JCMs through narrow pores, and how JCMs rotate near the pore entrance and inside short pores. Finally, conclusions are presented in section 4.

2. MATHEMATICAL MODEL AND NUMERICAL IMPLEMENTATION

2.1. Model for Self-Diffusiophoresis. To focus on the dynamics of JCMs driven by self-diffusiophoresis, we considered spherical JCMs of radius R_{JCM} submerged in a solution (see Figure 1). The JCMs are half-coated by catalysts that break down fuels in solution by chemical reaction. The reaction generates a concentration gradient of the reaction product along the JCM's surface. Such a concentration gradient induces an imbalance of interfacial forces near the JCM's surface, thus driving the self-diffusiophoresis of JCM. In practice, platinum is often used as catalytic material. If hydrogen peroxide is used as fuel, the product of the catalytic reaction is oxygen. Other fuels,[32,33] which lead to different

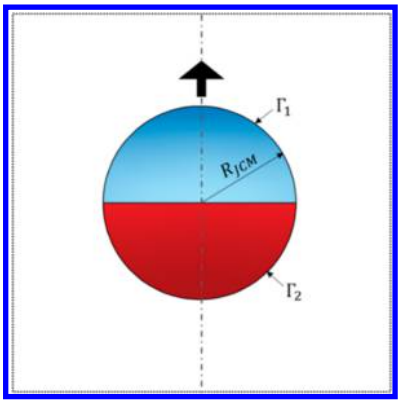

Figure 1. Schematic of the JCM. Half of the JCM's surface (Γ_2, colored in red) is coated with catalyst, while the other half of the JCM (Γ_1, colored in blue) exhibits no catalytic reactivity. The large black arrow indicates the swimming direction of JCM due to self-diffusiophoresis when the product of the catalytic reaction interacts repulsively with the JCM.

reaction products, can also be used. Here, to reduce the numerical difficulty, we neglect the transport of fuel and assume the concentration of fuels does not deviate from the initial concentration notably in our simulations. This treatment is valid when the Damköhler number Da is small. Da is the ratio of the diffusion and reactive time scales, i.e., $Da = s\bar{L}/D_f C_f$, where s is the rate at which fuels are consumed on the catalytic surface, $\bar{L}$ is the characteristic length scale involved in the supply of fuel to the catalytic surface, and D_f and C_f are the diffusion coefficient and concentration of fuel molecules, respectively. We focus our study in the regime of $Da \ll 1$. Hence, the transport of the fuel does not need to be solved. The effect of fuel transport will be studied in the future.

To describe the above self-diffusiophoresis of JCMs, we adopt the general model established previously.[10,30,31,34] Briefly, two sets of equations govern the reaction/transport of the reaction products and the movement of the fluids and the JCM. The concentration field of the reaction product (e.g., oxygen), c, is governed by the convection−diffusion equation

$$\frac{\partial c}{\partial t} + \boldsymbol{u}\cdot\nabla c = \nabla\cdot(D\nabla c) \tag{1}$$

where D is the diffusion coefficient of the reaction product and $\boldsymbol{u}$ is the fluid velocity. The neutral (noncatalytic) surface of the JCM (i.e., Γ_1 in Figure 1) is an impermeable wall, i.e.

$$-D\nabla c(\boldsymbol{x}, t)\cdot\boldsymbol{n} = 0 \qquad \text{on } \Gamma_1 \tag{2}$$

where $\boldsymbol{n}$ is the unit normal vector of the surface. The generation of reaction products is taken into account through the boundary condition imposed on the catalytic surface (i.e., Γ_2 in Figure 1)

$$-D\nabla c(\boldsymbol{x}, t)\cdot\boldsymbol{n} = \alpha \qquad \text{on } \Gamma_2 \tag{3}$$

where α is the rate at which reaction products are generated on the catalytic surface.

We note that, with a few exceptions,[30,35] the transient and convection terms in eq 1 were neglected in most prior studies of self-diffusiophoresis. This is justified for self-diffusiophoresis in bulk solution or near semi-infinite walls. However, these terms cannot be neglected when the JCM is confined inside narrow pores. Specifically, inside a narrow pore, the reaction product generated on the JCM surface must diffuse out of the

DOI: 10.1021/acs.langmuir.6b01214
Langmuir 2016, 32, 5580−5592

pore through its two ends. If the pore is not very short, the reaction product will gradually accumulate inside the pore before the JCM moves out of the pore. Indeed, the time scale required for dissipating the reaction product from a narrow pore to its surrounding is $\sim L_p^2/D$ (L_p is the pore length). Comparing this time scale with the time scale for the JCM to translocate the pore (i.e., L_p/U, where U is the JCM's characteristic velocity), we get a Péclet number $Pe_p = L_pU/D$. For not very short pores, $Pe_p \ll 1$ is not satisfied; hence the left-hand side of eq 1 cannot be neglected.

The fluids are modeled as incompressible and Newtonian. Since the Reynolds number is small, the inertia effect is negligible. Thus, the flow field is governed by

$$\nabla \cdot \boldsymbol{u} = 0 \tag{4}$$

$$\rho \frac{\partial \boldsymbol{u}}{\partial t} = -\nabla p + \mu \nabla^2 \boldsymbol{u} \tag{5}$$

where ρ and μ are the density and viscosity of the solution, and p is the pressure. The self-diffusiophoresis of JCM induced by the concentration gradient of reaction product is captured by imposing a phoretic slip on its surface.[31] This treatment is valid in the thin interaction layer limit,[30] i.e., $\lambda/L_c \ll 1$, where λ is the range of the interactions between the reaction product molecules (RPMs) and the JCM. L_c is the critical length scale in the diffusiophoresis process, e.g., the radius of the JCM (when JCM is in bulk solution) or the distance between the JCM surface and the surface of other JCM or walls. Typically, λ is of molecular dimension while L_c is hundreds of nanometers or larger. Hence $\lambda/L_c \ll 1$ holds in most situations. In principle, the transient term in eq 5 can be removed because the Reynolds number is much smaller than 1. Here, we keep this term because, with the ALE implementation in the code we used, having a time-dependent velocity makes updating the mesh easier. Keeping this term does not affect the result; e.g., the terminal velocity of a JCM in bulk solution predicted in our simulation agrees well with analytical solutions (see below).

With the above treatment, the fluid velocity on the JCM's surface is given by[30]

$$\boldsymbol{u}(\boldsymbol{x}, t) = \boldsymbol{U} + \boldsymbol{\omega} \times (\boldsymbol{x}_s - \boldsymbol{x}_0) + \boldsymbol{u}_s \qquad \text{on } \Gamma_1 \text{ and } \Gamma_2 \tag{6}$$

$$\boldsymbol{u}_s = M(\boldsymbol{I} - \boldsymbol{nn}) \cdot \nabla c \tag{7}$$

where $\boldsymbol{U}$ and $\boldsymbol{\omega}$ are the JCM's translational and rotational speed, $\boldsymbol{x}_s$ and $\boldsymbol{x}_0$ are the spatial position for the JCM surface and center, respectively. $\boldsymbol{u}_s$ is the phoretic slip velocity. $\boldsymbol{I}$ and M are the identity tensor and surface phoretic mobility. The mobility is given by[10]

$$M = k_B T \lambda^2/\mu \tag{8}$$

where k_B is the Boltzmann constant and T is the absolute temperature. For locally attractive/repulsive interactions between the reaction product and the JCM, the mobility M is negative (positive). We note that using the boundary condition given in eq 7 does not create inconsistency even in the presence of the transient and convection terms in eq 1 as long as $Pe\lambda/R \ll 1$, where Pe is the Péclet number based on the particle radius.[30,35]

The translation and rotation of the JCM are governed by

$$m_{JCM} \frac{d\boldsymbol{U}}{dt} = \boldsymbol{F}_H \tag{9}$$

$$I_{JCM} \frac{d\boldsymbol{\omega}}{dt} = \boldsymbol{T}_H \tag{10}$$

where m_{JCM} and I_{JCM} are the mass and the moment of inertia of JCM, respectively. $\boldsymbol{F}_H$ and $\boldsymbol{T}_H$ are the force and torque exerted on the JCM by the fluids given by

$$\boldsymbol{F}_H = \int_{\Gamma_1 \cup \Gamma_2} \boldsymbol{\sigma}_H \cdot \boldsymbol{n}\, dS = \int_{\Gamma_1 \cup \Gamma_2} (-p\boldsymbol{I} + \mu(\nabla \boldsymbol{u} + (\nabla \boldsymbol{u})^T)) \cdot \boldsymbol{n}\, dS \tag{11}$$

$$\boldsymbol{T}_H = \int_{\Gamma_1 \cup \Gamma_2} (\boldsymbol{x}_s - \boldsymbol{x}_0) \times (\boldsymbol{\sigma}_H \cdot \boldsymbol{n})\, dS \tag{12}$$

where $\boldsymbol{\sigma}_H$ is the hydrodynamic stress tensor. We note that, except for the very short time period when the JCM accelerates from zero velocity to a finite velocity, the net force and torque acting on the JCM are practically zero. This is consistent with the fact that the acceleration of the JCM is small for most of the time and the Reynolds number is close to zero. In addition, simulations in which the mass of JCM is reduced by 50% produced identical results, which confirms the fact that the force-free condition is met.

For the transport of JCMs in confined pores, the initial and boundary conditions for the reaction product concentration and fluid velocity must also be specified. Since these conditions are specific to each system to be studied, they are presented separately in section 3.

2.2. Numerical Implementation and Validation. To solve eqs 1−11 simultaneously and thus predict the self-diffusiophoresis of JCMs, the commercial finite element package COMSOL was used.[36] The ALE method[37] was utilized to handle the movement of JCM and the evolution of reaction product concentration and flow fields, as has been done for simulation of electrophoresis of colloidal particles.[38] The computational domains were discretized using triangular elements, and mesh was locally refined near the JCM surface and other solid boundaries (if present). During each simulation, multiple remeshing was typically performed to maintain the mesh quality. Mesh studies were also performed to ensure that the results are independent of the mesh size.

We first investigated the translation of JCM in bulk hydrogen peroxide solutions, because this is a well-studied case, and compare our numerical solution to the analytical prediction by Howse et al.[10] Specifically, a spherical JCM with a radius of 1 μm was placed in the middle of a hydrogen peroxide (H_2O_2) solution measuring 100 μm in radius and 200 μm in height, so that the JCM is effectively in a free solution. Oxygen is produced on the catalytic surface of the JCM at a constant rate of[10]

$$\alpha = \alpha_2 \frac{[H_2O_2]_v}{[H_2O_2]_v + \alpha_2/\alpha_1} \tag{13}$$

where $\alpha_1 = 4.4 \times 10^{11}$ μm^{-2} s^{-1}, $\alpha_2 = 4.8 \times 10^{10}$ μm^{-2} s^{-1}, and $[H_2O_2]_v$ is the volume fraction of the fuel (H_2O_2) in the liquid solution. We take the mobility M to be 1.011×10^{-36} m^5/s, consistent with previous reports.[31] Initially, the fluids and the JCM are both stationary and the concentration of reaction product (oxygen) is zero everywhere. On the outer boundaries of the liquid solution, the zero stress condition was imposed for the fluid flow and the zero concentration condition was enforced for the reaction product. The self-diffusiophoresis of the JCM was simulated in the axisymmetric domain occupied

DOI: 10.1021/acs.langmuir.6b01214
Langmuir 2016, 32, 5580−5592

by the liquid solution using the aforementioned model. During the simulation, the JCM reaches a steady velocity quickly (before it translates by 0.5 μm). The steady translation velocity for this problem has been predicted analytically as[10]

$$U_a = \frac{M\alpha}{4D} \tag{14}$$

Using the typical properties of O_2 and H_2O_2 solution ($D_{O_2} = 2 \times 10^{-9} m^2/s$, $\rho_{H_2O_2} = 1.05 \times 10^3$ kg/m^3, $\mu_{H_2O_2} = 1.02 \times 10^{-3}$ Pa·s), we compute the steady translation velocity of a JCM in a free solution. Figure 2 shows that the translation velocity predicted by our simulation agrees with that predicted by eq 14 very well.

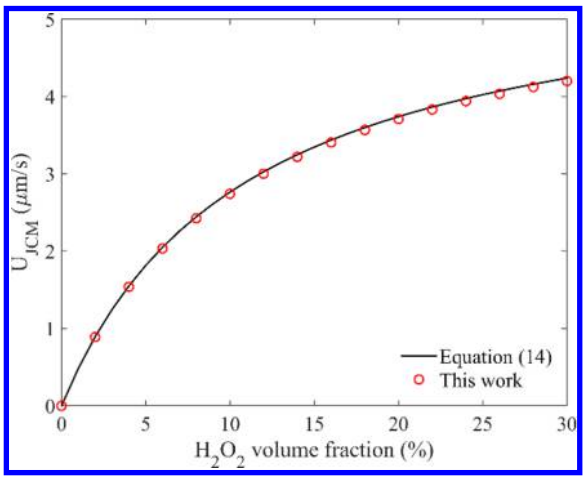

Figure 2. Diffusiophoresis velocity of a single JCM in bulk hydrogen peroxide solution predicted by analytical model (eq 14) and numerical simulations.

Since we will study how confinement affects the dynamics of JCMs in this work, we next verify that our numerical implementation is capable of capturing dynamics of particles under geometrical confinement. We simulated the passive diffusiophoresis of a noncatalytic sphere inside a cylindrical pore (see Figure 3, inset). Specifically, a sphere with a radius of R_s is positioned on the axis of a long, cylindrical pore with a radius of R_p and a length of L_p. The no-slip boundary condition is applied on the pore wall for the fluid velocity. If a concentration difference of a certain solute, Δc, exists at the pore's two ends, the sphere migrates along the pore axis via diffusiophoresis at a speed of[39]

$$U_p = \frac{M\Delta c}{L_p}\left[1 - 1.290\left(\frac{R_s}{R_p}\right)^3 + 1.896\left(\frac{R_s}{R_p}\right)^5 - 1.028\left(\frac{R_s}{R_p}\right)^6 + O\left(\left(\frac{R_s}{R_p}\right)^8\right)\right] \tag{15}$$

where M is the diffusiophoresis mobility of the sphere. Physically, as the particle radius R_s approaches R_p, the velocity reduces due to the confinement effects. In our simulations, a sphere with $R_s = 1$ μm was placed in the middle of a cylindrical pore with $R_p = 2-20$ μm. The length of the pore is $L_p = 40R_s$, the mobility M is 1.011×10^{-36} m^5/s, and Δc is 1 mol/m^3. Figure 3 compares the sphere's normalized translation velocity $U^* = U_pL_p/M\Delta c$ in pores with various radii as predicted by our simulations and by eq 15. The good agreement between the computed translation velocity and the analytical solution verifies that the numerical methods and codes used here are accurate for simulation of diffusiophoresis of particles in confined geometries.

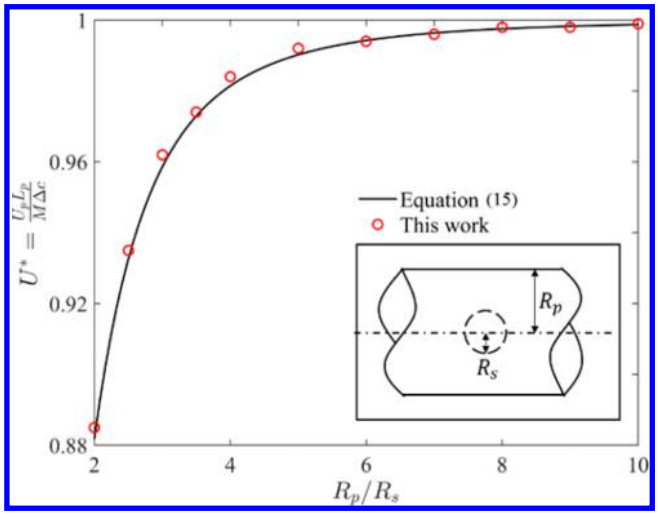

Figure 3. Passive diffusiophoresis velocity of a sphere in a long pore computed using simulations and using the analytical solution (eq 15). Inset is a schematic of the simulation model.

3. RESULTS AND DISCUSSION

Using the mathematical model and numerical method introduced above, we studied the self-diffusiophoresis of JCMs under confined conditions. Both the translational and rotational dynamics of JCMs were examined to understand how confinement affects the dynamics of JCMs.

3.1. Translocation of a Single Spherical JCM through a Short Pore. Here, we study the effect of confinement on the self-diffusiophoresis of spherical JCMs along the axis of a short cylindrical pore. The system consists of a spherical JCM (radius R_{JCM}, 1 μm; catalytic surface facing downward) and a cylindrical pore (radius, R_p; length, L_p) connected to two large reservoirs (see Figure 4). The diffusiophoresis mobility of the JCM, M, is 1.011×10^{-36} m^5/s. The rate of reaction production generated on the JCM's catalytic surface is 0.05 mol/m^2·s. At $t < 0$, the center of the JCM is fixed at a distance of R_{JCM} from the pore's entrance. Fluids inside the system are at rest and free of reaction product. Note that, since the diffusion length of the reaction product per unit time is far larger than the distance from the JCM to the confining walls, the flow and reaction product concentration fields near the JCM positioned at pore entrance reach steady state at a time scale much shorter than the time scale associated with their diffusiophoresis through the pore. Hence, the initial conditions barely affect the transport of JCM. At $t = 0$, the JCMs start moving by self-diffusiophoresis. The reservoir boundaries were treated as free of hydrodynamic stress and reaction products. The no-slip and no-flux boundary conditions were enforced on the pore walls. In principle, there can exist phoretic slips on the pore wall due to the concentration gradient of the reaction products. Depending on the interactions between reaction product and pore wall and the local reaction product concentration gradient, such a phoretic slip can be in the same or opposite direction of the JCM's diffusiophoresis. This can lead to rich JCM transport

DOI: 10.1021/acs.langmuir.6b01214
Langmuir 2016, 32, 5580−5592

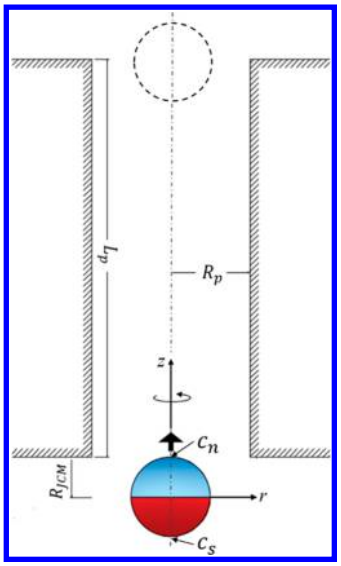

Figure 4. Schematic of a JCM translocating through a narrow pore. The JCM, with its catalytic surface facing the negative z-direction, is initially positioned at a distance of R_{JCM} from the pore's entrance. The large black arrow indicates the swimming direction of the JCM due to self-diffusiophoresis. The c_s and c_n are the product concentrations at the south and north poles of JCM, respectively.

behavior in the pore, similar to the situation when electrophoresis of particles in pores is affected by electroosmotic flows near walls.[39,40] Here, in order to focus on the confinement effect, we neglect these complications and assume that the diffusiophoretic slips on the pore wall are fully suppressed (e.g., by polymer coating).[41]

To study effects of confinement on JCM translation, we vary both R_p and L_p systematically. We first examine the effect of R_p by varying $\beta_W = R_p/R_{JCM}$ from 1.6 to 6, while keeping the pore length constant at $\beta_L = L_p/R_{JCM} = 20$. Hereafter, all variables are presented in dimensionless form. The velocity of the JCM U^* is scaled by the JCM's velocity in unbounded free solution, U^{∞}_{JCM}, and the JCM traveling distance Z^* is scaled by $L_t = L_p + R_{JCM}$, i.e., the distance traveled by the JCM when it fully translocates the pore (see Figure 4). With these choices of reference length and velocity, the dimensionless time is constructed as $\tau = tU^{\infty}_{JCM}/L_t$, where L_t/U^{∞}_{JCM} represents the time for a JCM to travel L_t in free solution. Figure 5a shows the translation velocity of the JCM through various pores as a function of time. In all cases, after self-diffusiophoresis is enabled ($\tau = 0$), the JCM quickly achieves a velocity close to its steady velocity in free solution (i.e., $U^* = 1$). In a moderately narrow pore ($\beta_W = 2$), the evolution of the JCM's velocity shows three distinct stages (see Figure 5a,b): when the JCM starts to enter the pore, its velocity decreases, reaching a minimum at $\tau < 0.25$; as the JCM moves deeper inside the pore and toward the exit, its velocity increases and reaches a maximum before exiting the pore; as the JCM reaches the exit (marked using plus signs in Figure 5b), its velocity decreases rapidly toward its steady-state velocity in the free solution. To understand such a nonmonotonic evolution of the JCM velocity, we note that the diffusiophoresis of JCM is governed by the phoretic slip on its surface, which in turn depends on the gradient of the RPM along its surface. Since the latter gradient depends qualitatively on the difference of the RPM concentrations $\Delta c_{sn} = c_s - c_n$ at the catalytic south pole c_s and uncoated north pole c_n (see Figure 4), we now examine this

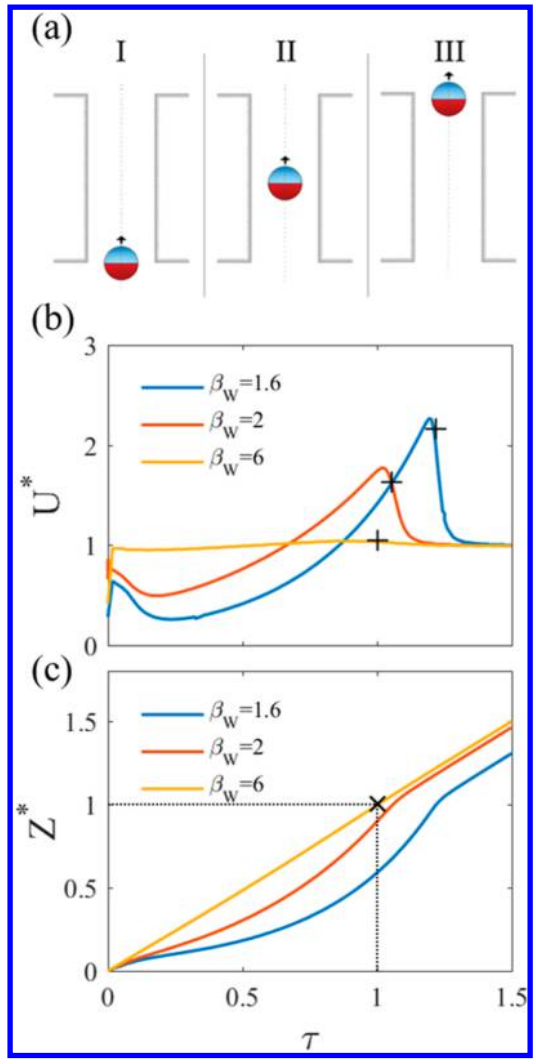

Figure 5. Translocation of a JCM through cylindrical pores with different radii but the same length ($L_p = 20R_{JCM}$). (a) Position of the JCM inside the pore at three time instants. (b, c) Evolution of JCM dimensionless velocity and JCM dimensionless traveling distance as the JCM "swims" through the pore. The plus signs in (b) mark the time instants at which the JCM leaves the pore. A JCM completes its translocation through the pore when it reaches $Z^* = 1$, and the corresponding time instant is marked by "×" in (c). Movie 1 in the Supporting Information shows the translocation of a JCM through a pore with $\beta_W = 1.6$.

difference and its evolution with time in Figure 6. Note, in all figures, Δc_{sn} is normalized by the difference of the product concentrations at the south and north poles of a JCM in free solution, Δc^{∞}_{sn}. The c_s and c_n are normalized by the product concentration at the north pole of a JCM in free solution, c^{∞}_n.

Figure 6b shows that, for $\beta_W = 2$, when the JCM just enters the pore, Δc^*_{sn} decreases, which is consistent with the gradual decrease of U^* observed in Figure 5a. As the JCM moves into the pore, the concentrations of reaction product at both its south and north poles increase because the diffusion of the RPMs toward the reservoir is hindered by the pore walls, leading to a buildup of RPMs on the JCM surface (see Figure 6a). However, c^*_s (solid lines) increases slower than c^*_n (dashed lines). This is because the transport of RPMs away from the south pole of a JCM, which faces a large reservoir nearby, is more efficient than from the north pole, which faces the interior

DOI: 10.1021/acs.langmuir.6b01214
Langmuir 2016, 32, 5580−5592

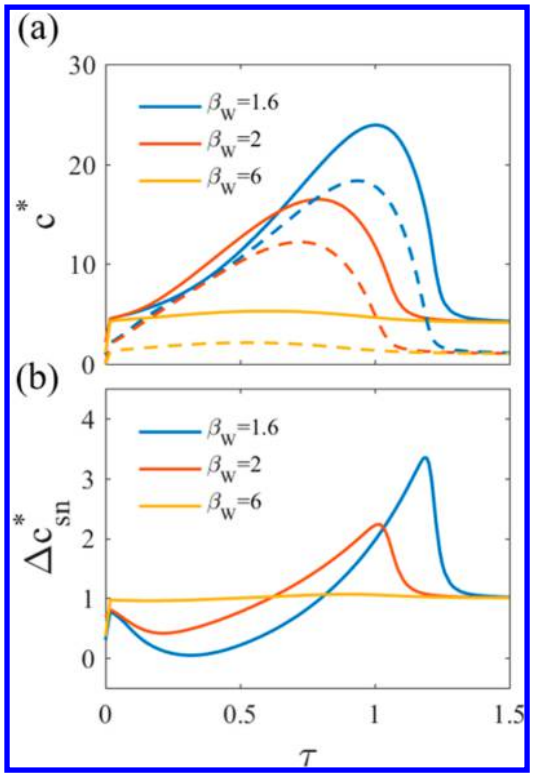

Figure 6. Reaction product concentrations at the south and north poles of the JCM. The evolution of c_s^* (solid lines) and c_n^* (dashed lines) (a), and the difference of reaction product concentrations at the south and north poles of the JCM (b) as the JCM "swims" through the pore.

of a long pore (see Figure 5a, I). Consequently, Δc_{sn}^* decreases as the JCM moves toward the pore interior (see Figure 6b) and the self-diffusiophoresis of JCM weakens. In response, JCM slows down. However, as the JCM moves deeper into the pore (see Figure 5a, II), Δc_{sn}^* increases because the product molecules generated on the catalytic surface are confined more near the catalytic surface and transported less to the uncoated surface due to the confinement by pore walls. Consequently, the JCM speeds up as shown in Figure 5b. Finally, when the JCM starts to move out of the pore (see Figure 5a, III), the concentration of reaction products near its south pole drops rapidly due to their efficient transport toward the large reservoir, leading to a rapid decrease of Δc_{sn}^* and the JCM velocity toward their values in free solutions. We note that the fact that confinement modifies the reaction product concentration field near JCMs in pores has been reported by Tao and Kapral.[21] In their work, the accumulation of reaction product inside the pore was removed using an artificial scheme in which reaction products are converted back to reactants when they diffuse far enough away from the catalytic dimer. As such, the effect of confinement on reaction product concentration is much less distinct in their studies.

When the pore becomes narrower (β_W = 1.6), the effect of confinement on the transport of RPMs becomes stronger and Δc_{sn}^* exhibits a much larger variation as the JCM enters and leaves the pore (see Figure 6b). These variations of Δc_{sn} modify the translation of JCM through the same physics discussed above, but the effects are more pronounced; e.g., the maximal speed of the JCM, which is achieved when the JCM is about to exit the pore, is 2.25 times that in free solutions (see Figure 5b). On the other hand, as the pore becomes wider (β_W = 6), the effect of confinement on JCM dynamics diminishes: the velocity of the JCM changes only slightly as the JCM passes through the pore and the JCM velocity and the translocation time are hardly affected by the presence of the pore walls (see Figure 5b,c).

Overall, the translocation of JCMs through the pore is slowed down rather modestly by the confinement. In fact, the slowdown of self-diffusiophoresis by confinement is weaker compared to that for the particle transport driven by other well-known mechanisms. Figure 7 compares the average speed of

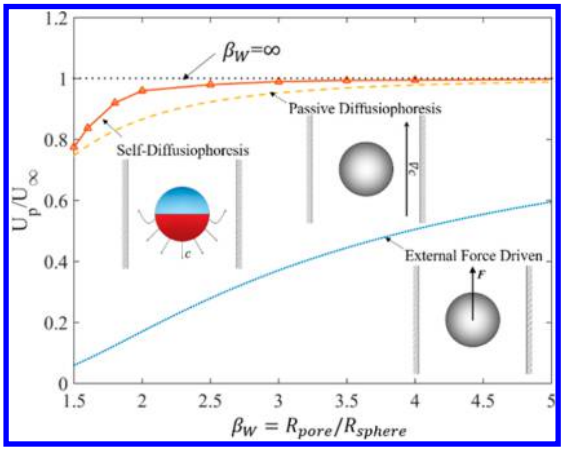

Figure 7. Comparison of the average speed of sphere through pores driven by different mechanisms as a function of confinement $\beta_W = R_p/R_s$ (R_p and R_s are the radii of the pore and sphere, respectively). For each transport mechanism, the average speed of the sphere inside a pore U_p is scaled using the sphere's speed in the free solution, U_∞. Insets are the sketches of different particle transport mechanisms.

spheres traveling through narrow pores driven by self-diffusiophoresis, external body forces,[42] and passive diffusiophoresis.[40] In the latter two cases, the motion of a sphere is induced by an external body force and an externally imposed concentration gradient of a certain solute (see the insets of Figure 7), respectively. For the self-diffusiophoresis of a sphere through a short pore, its average speed is defined as the mean velocity during its translocation through the pore. For transport by the latter two mechanisms, the pore is infinitely long and Stokes flow is assumed; for self-diffusiophoresis, the pore length is fixed at $20R_{JCM}$. The comparison of the transport of particles driven by different mechanisms is complicated by the fact that the mean velocity of a JCM driven by self-diffusiophoresis is obtained in a finite-length pore, which includes the "entrance" and "end" effects. Nevertheless, since these effects tend to cancel each other (cf. Figure 5a), the above comparison can still lead to useful insight on how confinement affects the transport of particles by different mechanisms.

Figure 7 shows that, for β_W = 2, the velocity of a sphere driven by external force is 82% smaller than that in free solutions. Such a significant slowdown is caused by the enhanced hydrodynamic drag in narrow pores.[42] For the passive diffusiophoresis in the same pore, its speed decreases less significantly, by 11%. This is because, for a given externally imposed concentration gradient of solutes (usually imposed at a distance away from the sphere), the solute concentration gradient near the sphere is greatly enhanced when it is confined inside a pore. This enhances the phoretic driving force and counteracts the enhanced hydrodynamic drag caused by confinement.[43] For self-diffusiophoresis of a JCM in the same

DOI: 10.1021/acs.langmuir.6b01214
Langmuir 2016, 32, 5580−5592

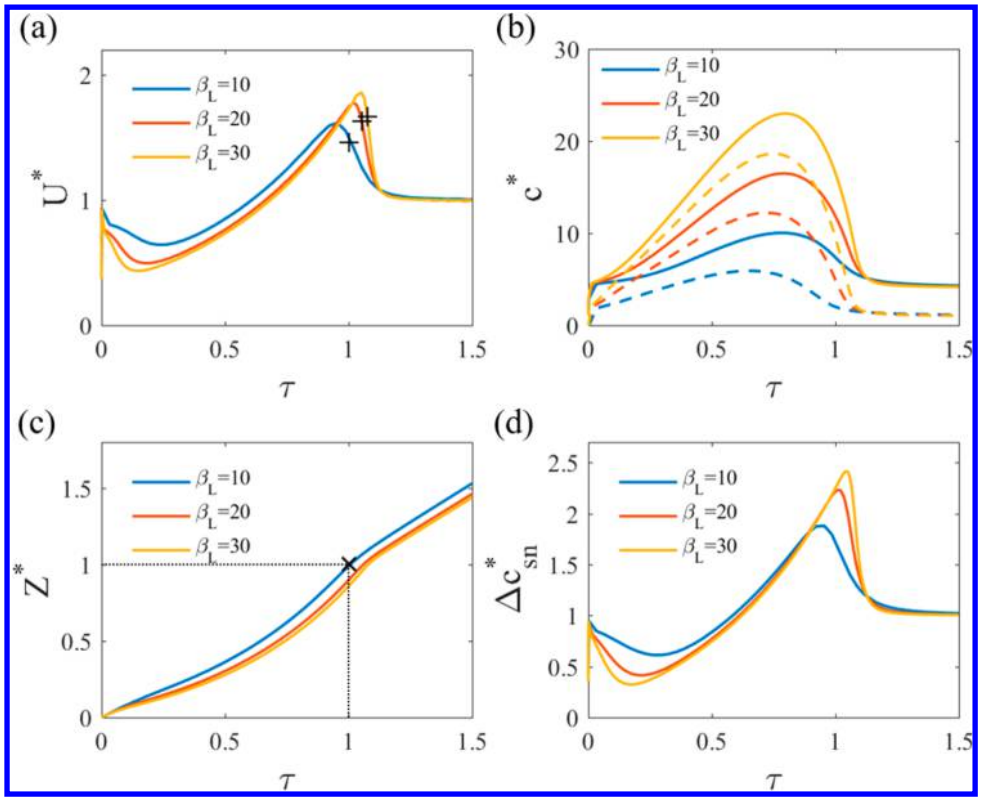

Figure 8. Translocation of a JCM through cylindrical pores with different lengths but the same radius ($R_p = 2R_{JCM}$). The evolution of JCM dimensionless velocity (a), the c_s^* (solid lines) and c_n^* (dashed lines) (b), JCM dimensionless position (c), and the difference of reaction product concentrations at the south and north poles of the JCM (d) as the JCM "swims" through the pore.

pore ($\beta_W = 2$), the slowdown by confinement is even weaker (~4%). This can be understood as follows. First, since the RPMs are generated on the JCM's catalytic surface and they must diffuse toward the two ends of the pore; their concentration near the JCM's catalytic surface increases when the pore size reduces. This tends to enhance the concentration gradient of reaction product on the JCM's surface more greatly compared to the situation in passive diffusiophoresis. Second, for the translocation of JCM through a short pore by self-diffusiophoresis, the JCM travels faster than in free solution when it approaches the pore's exit, which partially compensates the slowdown of JCM near the pore entrance (see Figure 5b). Since this feature is absent for passive diffusiophoresis of a sphere in a long pore, the overall slowdown is weaker for self-diffusiophoresis. Finally, the fact that particle−wall hydrodynamic interactions have a longer range in force-driven particle transport than those in classical and self-diffusiophoresis also contributes to the stronger sensitivity of force-driven particles to the confinement by pore walls. Figure 7 also shows that, when a pore becomes very narrow (e.g., $\beta_W = 1.5$), the average speed of particle transport by self-diffusiophoresis becomes similar to that by passive diffusiophoresis. This is likely because, for very narrow pores, the pore entrance greatly slows down the JCM as it enters the pore (see Figure 5b), hence the JCM takes longer time to translocate the pores. On the other hand, the passive diffusiophoresis of particle is measured inside infinitely long pores and, therefore, is not affected by such an entrance effect. From the above discussions, it is clear that the self-diffusiophoresis of JCMs in confined geometries exhibits interesting new features compared to other forms of particle transport in similar geometries. Identifying and understanding these features are useful for improving the performance of microsystems in which self-diffusiophoresis is used for particle transport.

We next examine the effect of pore length L_p on the JCM translocation through pores by varying $\beta_L = L_p/R_{JCM}$ between 10 and 30, while fixing $\beta_W = 2$. Figure 8a shows that, in all pores, the three stages of JCM translocation, during which the JCM velocity varies nonmonotonically, are still observed. In longer pores, the initial slowdown of JCM is more significant, consistent with the greater decrease of Δc_{sn}^* in the longer pores during this stage (see Figure 8d). The latter is mostly caused by the fact that, in longer pores, RPMs build up more easily near the north pole of the JCM (see Figure 8b), which faces the interior of the pore. In longer pores, the increase of the JCM speed once it is deep inside the pore is also more obvious. For example, the maximal velocity of the JCM inside a pore increases by 15% when β_L increases from 10 to 30. This is because, in longer pores, the buildup of the RPMs near the catalytic surface is more significant due to the less effective transport of these molecules from these pores to reservoir and the longer time the JCM spends inside these pores. Overall, Figure 8c shows that, in moderately narrow pores ($\beta_L = 2$), the average speed of the JCM decreases only slightly as the pore becomes longer: as β_L increases from 10 to 30, the time for JCM to translocate through the pore increases by 8%, i.e., the average speed of the JCM inside the pore decreases by 8%.

We also studied how the reaction rate on the JCM's catalytic surface affects its translocation through pores (see Figure S1 in the Supporting Information). We found that, for a given pore, the average translocation velocity roughly increases linearly with the reaction rate. Equation 14 shows that, in bulk solutions, the velocity of a JCM also increases linearly with the reaction rate. The fact that confinement does not greatly

DOI: 10.1021/acs.langmuir.6b01214
Langmuir 2016, 32, 5580−5592

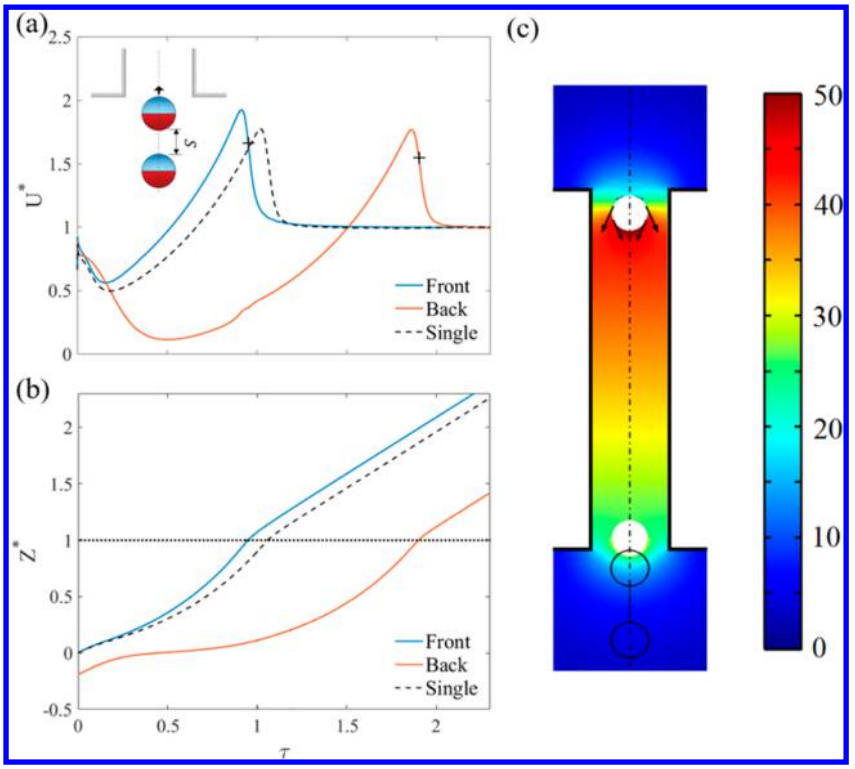

Figure 9. Translocation of a pair of JCMs through a short pore. (a, b) Evolution of the velocity (a) and the position (b) of each JCM as a function of time. The dashed line is the result of single JCM translocating through the same short pore from Figure 5. A JCM completes its translocation through the pore when it reaches $Z^* = 1$. (c) Reaction product concentration field at $\tau = 0.9$, when the front JCM is about to exit the pore (the JCMs are marked by the white circles). The black circles denote the initial positions of the JCMs. The arrows denote the slip velocity on the JCMs' surface. Movie 2 in the Supporting Information shows the translocation process.

change the effect of reaction rate on the JCM movement is likely because the effect of confinement on the transport of reaction product is similar regardless of the reaction rate.

The above discussion revealed that the translocation of JCMs through pores is governed by the complex interplay between hydrodynamics in confinement and the transport of reaction products near the JCM and inside the pores. The weak dependence of the JCM's average translocation speed on the pore size and length is due to the rather strong cancellation effects of these processes. From an application perspective, the fact that a JCM's average translocation speed is affected weakly by confinement of pore walls helps simplify its design for transport in pores because its velocity in free solutions can be used to estimate its translocation. It should, however, be cautioned that these results are obtained under the condition that the reaction rate is a constant; i.e., the effect of consumption of fuel on the reaction rate is assumed to be small. As discussed earlier, this assumption is reasonable when $Da = s\bar{L}/D_fC_f \ll 1$. Because the pore length is the most relevant length scale for fuel transport inside a pore, it follows that the above results on JCM dynamics in pores hold for pores with pore length smaller than D_fC_f/s. For much longer pores, the effects of fuel transport must be considered in analyzing the JCM dynamics.

3.2. Translocation of a Pair of Spherical JCMs through a Short Pore. In practical applications and many recent experiments, many JCMs could coexist in the system.[6,44,45] Because of the "crowding" of JCMs in these systems, the dynamics of individual JCMs can be affected greatly by the interactions between the JCMs. Here we consider the translocation of a pair of JCMs through a cylindrical pore to gain insights on how interactions between JCMs affect their transport in confinement. Specifically, two JCMs ($R_{JCM} = 1$ μm) are positioned near the entrance of a short cylindrical pore ($R_p = 2R_{JCM}$; $L_p = 20R_{JCM}$), with their axes aligned with the pore's axis. The pore is open to large liquid solution reservoirs (length, $50R_{JCM}$; radius, $50R_{JCM}$) at both ends. The distance between the center of the JCM closer to the pore and the pore entrance is R_{JCM}. The separation between the JCMs is $2R_{JCM}$, and the catalytic surfaces of both JCMs are facing downward (see Figure 9a, inset). The interactions between JCMs are relatively strong under these conditions, but we verified in separate simulations that varying the distance between JCMs does not qualitatively change the results. The initial conditions and boundary conditions are similar to those in section 3.1; e.g., the JCMs are at rest for $\tau < 0$ and allowed to move by self-diffusiophoresis at $\tau = 0$.

Figure 9a shows the evolution of the velocity of the two JCMs (hereafter, the JCM entering the pore first is termed the front JCM, while the other JCM is termed the back JCM) as they pass through the pore. The evolution of the velocity of both JCMs exhibits the same trend found during the translocation of single JCMs through the pore (dashed lines in Figure 9); i.e., as a JCM passes through the pore, the slowdown−speedup−slowdown cycle of its velocity is preserved qualitatively. There are, however, quantitative differences between the dynamics of the JCMs studied here and in Figure 5a. Compared to the situation when a single JCM passes through the pore, for the front JCM, its initial slowdown terminates at an earlier time, its subsequent speedup is more significant (Figure 9a), and its translocation time is ∼12% shorter (Figure 9b). For the back JCM, it slows down much

DOI: 10.1021/acs.langmuir.6b01214
Langmuir 2016, 32, 5580−5592

more greatly as it enters the pore and becomes nearly stalled; while its speed does increase later and nearly reaches the maximal velocity of a single JCM passing through the same pore (Figure 9a), its net translocation time is 50% longer than that of a single JCM passing through the pore (Figure 9b). Overall, pairing of JCMs affects the translocation of the front and the back JCMs very differently: it weakly accelerates the translocation of the front JCM, but greatly slows down the translocation of the back JCM.

The different behaviors of JCMs passing through a pore as pairs and as singlets and the different effects of JCM pairing on the translocation of the front and back JCMs originate mostly from the "chemical interactions" between a pair of JCMs translocating a pore. These chemical interactions originate from the modification of the slip velocity and viscous stress on the JCM's surface due to changes in the reaction product concentration field near the JCM. They have been previously shown to affect the dynamics of a pair of "active" particles or a JCM near confining walls.[3,16,23−29,46] In light of these works, we analyze the reaction product concentration nearby in the system. Pairing of JCMs inside a narrow pore leads to a concentration field of the reaction product shown in Figure 9c. Because of pairing, the concentration of RPM near the catalytic surface of the front JCM is enhanced greatly, which enhances the strength of diffusiophoresis of the front JCM (see the phoretic slip velocity $\boldsymbol{u}_s$ indicated by the black arrows in Figure 9c). Meanwhile, the concentration of RPM near the noncatalytic surface of the back JCM is elevated by the pairing of JCMs, which weakens the phoretic slip on the surface of the back JCM and thus slows down its translocation. The "chemical interactions" between adjacent JCMs confined in narrow pores may be useful in designing a complex system for particulate transport; e.g., they may be harnessed to accelerate or block the motion of a certain group of particles, hence being useful for local control of system behaviors.

3.3. Rotational Dynamics of Circular JCMs near and in Short Pores. In free solutions, self-diffusiophoresis drives a JCM to move in the direction defined by the vector pointing from the apex of its catalytic surface to the apex of its noncatalytic surface. For convenience, we can identify this vector as the "phoretic axis" of the JCM (identified as $\boldsymbol{r}_{sn}$ in Figure 10). In the above discussions, all spherical JCMs are positioned with their phoretic axes coinciding with the pore's axis and thus they do not experience rotation. In practice, however, the phoretic axis of JCMs may not be fully aligned with the pore's axis, e.g., due to thermal fluctuations or forces imposed by external magnetic fields.[47] Therefore, it is important to understand how JCMs' orientation affects their transport into and through pores. Here, we study the transport of single JCMs in two scenarios in which their axes are not always fully aligned with the pore axis. Since simulation of particle transport in confined space, in which a particle can approach the pore wall closely, is expensive, all simulations are performed in two-dimensional spaces (i.e., JCMs are circular disks) to explore the JCMs' translation and rotational dynamics. We note that prior studies of the electrophoresis of charged particles in a microchannel revealed that the rotation of particles driven by phoretic effects can be indeed captured quite well in two-dimensional simulations.[48]

3.3.1. A JCM Entering a Pore. In this first scenario, a circular JCM is initially positioned at the entrance of a pore with its center on the pore's axis and its phoretic axis forming an inclination angle θ_0 with the pore's axis (identified as $\boldsymbol{r}_c$ in Figure 10). The JCM has a radius of R_{JCM} = 1 μm, and the pore has a width of $6R_{JCM}$ and a length of $50R_{JCM}$. Two large reservoirs are included at the pore's two ends. The pore walls are treated as no-slip and nonpermeable surfaces. At τ = 0, the entire system is free of RPM and both the fluids and the JCM have zero velocity. At τ > 0, the JCM is allowed to move by self-diffusiophoresis.

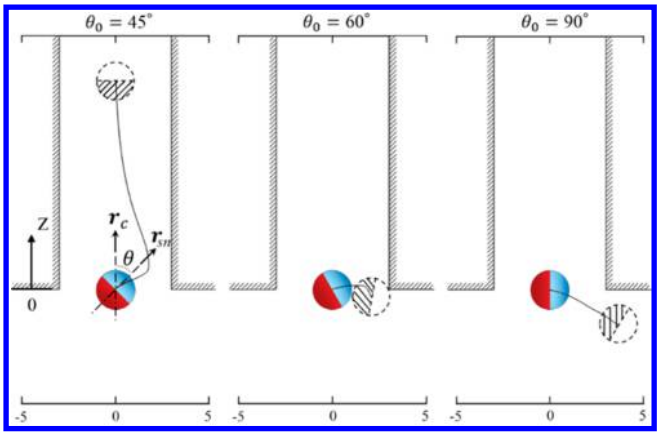

Figure 10. Trajectories of JCMs with different initial inclination angles θ_0 near a pore's entrance. The JCM's center is initially positioned at z = 0. For small θ_0, the JCM can rotate toward the pore interior and swim into the pore. For large θ_0, the JCM either collides with the pore wall or swim away from the pore. Movie 3 in the Supporting Information shows the trajectory of the JCM with θ_0 = 90°.

Figure 10 shows the trajectories of the JCMs with different initial inclination angles θ_0. We observed the dynamics of the JCM greatly depends on θ_0. For small θ_0 (e.g., θ_0 = 45°), initially, the JCM mostly moves toward the right pore wall with little rotation. Once it is close to the pore's right wall, the JCM rotates rapidly in the counterclockwise direction and turns into the pore and its phoretic axis becomes aligned with the pore's axis. The JCM's motion is somewhat similar to the "reflection" and "skimming" of JCMs near semi-infinite walls when they approach the wall at some inclination angles.[23,24,26,27,46] For large θ_0 (e.g., θ_0 = 60° and 90°), the initial stage of JCM movement is similar to that for small θ_0. However, by the time the JCM is close to the right pore wall, the JCM rotates in the clockwise direction. This rotation causes the JCM's phoretic axis to become less aligned with the pore's axis, and the JCM either collides with the pore entrance (θ_0 = 60°) or swims toward the reservoir (θ_0 = 90°).

To understand these observations, we note that the rotation of a JCM is determined by the net torque acting on it, which in turn depends on the distribution of the viscous stress on its surface (see eq 12). The viscous stress at any point on a JCM's surface scales as $\sigma_s \sim \mu u_t/l$, where u_t is the local fluid velocity tangential to the JCM's surface and l is the length over which the fluid velocity decays to zero as one moves away from the JCM's surface. For a JCM near pore walls, l can be taken as the distance from the JCM surface to the nearest wall, L_{sw}. Given that the velocity of fluids on the JCM surface is usually dominated by the phoretic slip velocity u_s, we have $\sigma_s \sim \mu u_s/L_{sw}$. The part of a JCM's surface on which the phoretic slip velocity u_s points in the counterclockwise (clockwise) direction with respect to its center experiences a local stress in the clockwise (counterclockwise) direction, and is defined as Γ_c (Γ_{cc}) and labeled by green (yellow) curves in Figure 11. As reported in previous studies, the local stress on JCM's surface is

DOI: 10.1021/acs.langmuir.6b01214
Langmuir 2016, 32, 5580−5592

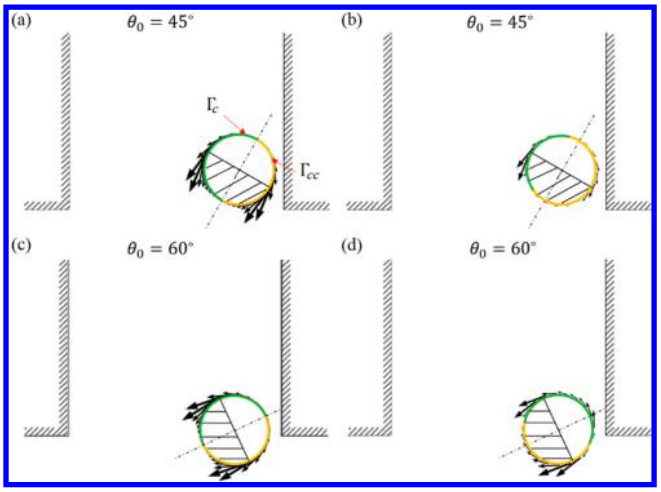

Figure 11. Distribution of the phoretic slip velocity u_s on the surface of JCMs when they approach the pore wall. Each JCM is originally placed at the pore entrance with an inclination angle θ_0 as shown in Figure 10. The surface on which u_s points in the clockwise (counterclockwise) direction with respect to the JCM center and the local viscous stress causes a counterclockwise (clockwise) torque is defined as Γ_{cc} (Γ_c). In (a) and (c), u_s is taken, hypothetically, to be that for JCM in the free solution to isolate the hydrodynamic effect on JCM rotation. In (b) and (d), the real u_s determined in simulations is shown to help delineate the chemical effects on JCM rotation.

controlled by two effects: the chemical effect and the hydrodynamic effect.[23,24,26,46] The chemical effect refers to the fact that the viscous stress depends on u_s, which is determined by the tangential gradient of chemical species (in our case, the product of the catalytic reactions) on the JCM's surface as shown by eq 7. The chemical effect depends strongly on the transport of the reaction products, which is affected by the confinement by pore walls. The hydrodynamic effect refers to the fact that, for a given u_s, the local viscous stress depends on the fluid flow near the JCM's surface, or roughly the distance from the JCM surface to the nearest pore wall as pointed out above.

Both hydrodynamic and chemical effects contribute greatly to the dependence of a JCM's rotation on its initial inclination angle, θ_0. For clarity, we first examine purely the hydrodynamic effect. To this end, we assume that the phoretic slip velocity u_s (black arrows in Figure 11) on the surface of a JCM is identical to that when the JCM is located in unbounded free solution regardless its location and orientation in the system. When a JCM is placed at the entrance of the pore with $\theta_0 = 45°$, initially, the JCM swims toward the pore wall with little rotation. Once the JCM is near the pore wall (e.g., at $\tau = 0.34$, see Figure 11a), the viscous stress σ_s on the Γ_{cc} surface becomes larger than that on the Γ_c surface: while the slip velocity distribution on the Γ_{cc} and Γ_c surface is the same, L_{sw} is smaller on the Γ_{cc} surface than on the Γ_c because of the small inclination angle of the JCM. As a result, the net torque generated by the viscous stress on the Γ_{cc} surface is stronger than that on the Γ_c surface, and the JCM rotates in the counterclockwise direction. We next examine the role of chemical effects in the rotation of the JCM. To this end, recall that confinement affects the transport of reaction product near the JCM and thus the u_s distribution on JCM's surface. In Figure 11b, we plot the real u_s (black arrows) on the JCM's surface at $\tau = 0.34$. We observe that the area of the JCM's surface (yellow) on which u_s points to the clockwise direction is larger than the area of the JCM's surface (green) on which u_s points to the counterclockwise direction; i.e., Γ_{cc} is larger than Γ_c. The larger area of Γ_{cc} than Γ_c tends to increase the net torque exerted on the JCM in the counterclockwise direction, and thus the JCM rotates in the counterclockwise direction and swims deeper into the pore. Overall, the role of hydrodynamic and chemical interactions on the JCM dynamics in the situation examined here shows clear similarity with that for JCMs near semi-infinite walls.

For the JCM with an initial inclination angle of $\theta_0 = 60°$, we again first focus on the hydrodynamic effects only. Figure 11c shows the sketch of the JCM at $\tau = 0.24$, in which the slip velocity u_s on the JCM's surface is taken as that for JCM in free solution. In this case, because of its large θ_0, most of the Γ_{cc} surface faces the reservoir instead of the right pore wall and most of the Γ_c surface faces the pore interior, which are in sharp contrast to the situation for the JCM with $\theta_0 = 45°$ (see Figure 11a). As a result, the L_{sw} for the majority of the Γ_{cc} surface is larger than that for the majority of the Γ_c surface. Hence the viscous stress is stronger on the Γ_c surface than on the Γ_{cc} surface, and the resulting net torque drives the JCM to rotate in

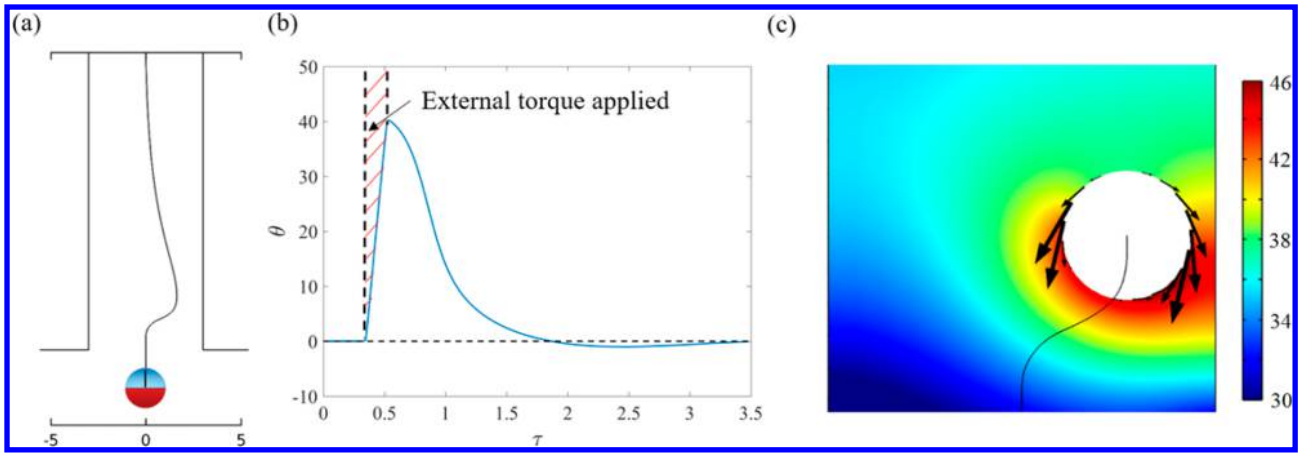

Figure 12. Self-alignment behavior of JCM swimming inside a pore. The JCM was initially placed near the pore entrance with phoretic axis fully aligned with the pore axis. An external, clockwise torque was applied on the JCM during $\tau = 0.34–0.52$ to rotate the JCM in the clockwise direction. (a, b) Trajectory (a) and inclination angle (b) of the JCM as a function of time. (c) Distribution of the reaction product near the JCM at $\tau = 0.87$. The black arrows denote the phoretic slip velocities on the JCM's surface.

DOI: 10.1021/acs.langmuir.6b01214
Langmuir 2016, 32, 5580−5592

the clockwise direction. We further consider the chemical effect by considering the real phoretic slip velocity u_s on the JCM surface (see Figure 11d). We observe that, compared to those shown in Figure 10c, the area of the Γ_c surface facing the pore interior/wall and the area of the Γ_{cc} surface facing the reservoir both increase. Consequently, the L_{sw} on the Γ_{cc} surface increases, while the L_{sw} on the Γ_c surface decreases. These changes enhance (reduce) the viscous stress on the Γ_c (Γ_{cc}) surface and increase the net torque acting on the JCM in the clockwise direction. Hence, the chemical effect further enhances the clockwise rotation of the JCM.

For $\theta_0 = 90°$, the mechanism of the rotational motion of JCM is similar to that for $\theta_0 = 60°$. The imbalance of stress distribution causes net, clockwise torque acting on the JCM and drives it to rotate in the clockwise direction. However, because of the larger initial inclination angle, the JCM swims toward the reservoir instead of colliding with the pore wall.

3.3.2. A JCM Swimming Inside a Pore. In this second scenario, we study how a JCM inside a pore rotates when its phoretic axis becomes misaligned with the pore axis. As shown in Figure 12a, initially a JCM swims toward a pore entrance with its phoretic axis fully aligned with the pore axis. At $\tau = 0.34$, when the JCM is inside the pore, an external torque is applied on the JCM for 1 s, forcing it to rotate in the clockwise direction. At $\tau = 0.52$, the inclination angle of the JCM reaches 40°. The external torque is then removed and the JCM swims solely by self-diffusiophoresis. This problem mimics the situation in which the JCM become misaligned with the pore axis due to reasons such as thermal fluctuations. The size of the JCM, the pore, and the reservoir are the same as those in the scenario 1.

Figure 12 shows the trajectory of the JCM and its inclination angle as a function of time. The JCM exhibits a self-alignment behavior after the external torque was removed: (1) it moves away from the right pore wall and its inclination angle decreases; (2) eventually, the JCM becomes centered across the pore with its phoretic axis aligned with the pore axis. The first observation is similar to that observed when a JCM approaches an open, planar wall with its phoretic axis initially forming an angle less than 90°.[23,24] This self-alignment behavior is a result of the combined chemical and hydrodynamic effects. When the JCM deviates from the pore axis and approaches the right pore wall as shown in Figure 12a, the distance between the JCM's surface facing the right wall decreases, and hydrodynamics effects cause the viscous stress $\sigma_s \sim \mu u_s/L_{sw}$ on this surface to increase. Meanwhile, the phoretic slip velocity on the JCM's surface facing the right wall increases due to chemical effects, and thus enhances the viscous stress on this surface. The increased viscous stress on the JCM's surface facing the right wall leads to a net counterclockwise torque acting on the JCM. Such a net torque drives the JCM to rotate in the counterclockwise direction so that its phoretic axis becomes more aligned with the pore axis. Moreover, when the JCM is close to the wall and rotating, it generates a high concentration zone for the reaction product near the wall (see Figure 12c). Such a high concentration zone triggers the horizontal diffusiophoresis of the JCM toward the pore center. Because of the rotation and horizontal movements, the JCM tends to swim away from the pore wall and thus exhibit the self-alignment behavior shown in Figure 12a,b.

The JCM's off-axis movement shown in Figure 12 bears some similarities with the off-axis motion (e.g., swinging and tumbling) of squirmers confined in pores.[49,50] Similar to the off-axis motion of JCMs, the modification of the viscous stress on the squirmer's surface as it moves toward the pore walls is essential for such motion.[49,50] The JCM in our study does not exhibit periodic motion such as swinging (i.e., approaching toward and departing from the pore axis periodically) but moves toward and then resides on the pore axis. This difference originates from the modification of the surface slip velocity by chemical effects, which plays an important role in JCM dynamics in narrow pores, and is not included in the squirmer models.

4. CONCLUSIONS

The translational and rotational dynamics of JCMs in confined geometries driven by self-diffusiophoresis were studied using direct numerical simulations. Our simulations revealed that JCMs can exhibit rich dynamic behavior under confined conditions. For the translocation of a single spherical JCM through a short cylindrical pore, while the JCM is slowed down by the pore on average, the speed of the JCM can exceed that in free solutions when the JCM approaches the pore exit. The overall slowdown of self-diffusiophoresis becomes more obvious when the pore size reduces, but its dependence on the pore size is much weaker than the transport of particles driven by external force or externally imposed concentration gradients. For the translocation of a pair of JCMs through a pore, when both of their catalytic surfaces are facing the bottom reservoir direction, the front JCM speeds up but the back JCM slows down. For a circular JCM near a pore entrance and with its phoretic axis not aligned with the pore axis, the JCM can enter the pore and its phoretic axis becomes fully aligned with the pore axis if its initial inclination angle is small. Otherwise, the JCM either collides with the pore entrance or moves away into the reservoir. For a JCM already inside a pore, self-diffusiophoresis can align the JCM's phoretic axis with the pore axis and drive it toward the pore center for the parameters considered here.

Analyses showed that these rich behaviors have both hydrodynamic and chemical origins. In particular, the modification of the chemical species concentrations surrounding a JCM by wall confinement and its neighboring JCMs, which can be called "chemical effect", plays a key role in determining the translation and rotation of the JCMs. In ordinary particulate transport problems, chemical species in the solution and their transport have little or no impact on the particulate transport. In the self-diffusiophoresis of JCMs, however, chemical effects become important because the gradient of chemical species on their surface impacts the phoretic slip velocity on the surface. These effects, already identified in studies of JCM dynamics near semi-infinite walls, are especially significant when the confinement is severe (e.g., when a JCM is inside a narrow channel[21]) or when JCMs approach each other closely.[16,28,29] Given these situations are increasingly encountered in the applications of JCMs, chemical effects should be taken into account in the design and operation of JCMs in these applications.

While our simulations captured the key physics of self-diffusiophoresis of JCMs, some other interesting physics are not considered. For instance, the effect of fuel transport on JCM dynamics is neglected. Likewise, possible diffusioosmotic flows induced by the charges on JCM/pore walls as well as the gradient of reaction product concentration on the pore wall are neglected. These effects merit additional exploration in future studies.

DOI: 10.1021/acs.langmuir.6b01214
Langmuir 2016, 32, 5580−5592

■ ASSOCIATED CONTENT

Supporting Information

The Supporting Information is available free of charge on the ACS Publications website at DOI: 10.1021/acs.langmuir.6b01214.

Effects of reaction rate on the translocation of a single JCM through a pore (PDF)

Translocation of a single JCM through a pore (AVI)

Translocation of a pair of JCMs through a pore (AVI)

Trajectory of a single JCM near the entrance of a pore (AVI)

■ AUTHOR INFORMATION

Corresponding Author

*E-mail: ruiqiao@vt.edu. Web: http://www.me.vt.edu/ruiqiao.

Notes

The authors declare no competing financial interest.

■ ACKNOWLEDGMENTS

The authors gratefully acknowledge support by the National Science Foundation (ECCS-1303134 and ECCS-1464146).

■ REFERENCES

(1) Ismagilov, R. F.; Schwartz, A.; Bowden, N.; Whitesides, G. M. Autonomous Movement and Self-Assembly. *Angew. Chem., Int. Ed.* **2002**, *41*, 652−654.

(2) Paxton, W. F.; Kistler, K. C.; Olmeda, C. C.; Sen, A.; St. Angelo, S. K.; Cao, Y. Y.; Mallouk, T. E.; Lammert, P. E.; Crespi, V. H. Catalytic Nanomotors: Autonomous Movement of Striped Nanorods. *J. Am. Chem. Soc.* **2004**, *126*, 13424−13431.

(3) Kapral, R. Perspective: Nanomotors without Moving Parts That Propel Themselves in Solution. *J. Chem. Phys.* **2013**, *138*, 020901.

(4) Ebbens, S. J.; Howse, J. R. In Pursuit of Propulsion at the Nanoscale. *Soft Matter* **2010**, *6*, 726−738.

(5) Kolmakov, G. V.; Yashin, V. V.; Levitan, S. P.; Balazs, A. C. Designing Self-Propelled Microcapsules for Pick-up and Delivery of Microscopic Cargo. *Soft Matter* **2011**, *7*, 3168−3176.

(6) Baraban, L.; Tasinkevych, M.; Popescu, M. N.; Sanchez, S.; Dietrich, S.; Schmidt, O. G. Transport of Cargo by Catalytic Janus Micro-Motors. *Soft Matter* **2012**, *8*, 48−52.

(7) Fukuyama, T.; Fuke, A.; Mochizuki, M.; Kamei, K.-i.; Maeda, Y. T. Directing and Boosting of Cell Migration by the Entropic Force Gradient in Polymer Solution. *Langmuir* **2015**, *31*, 12567−12572.

(8) Zhang, Z.; Zhao, A.; Wang, F.; Ren, J.; Qu, X. Design a Plasmonic Micromotor for Enhanced Photo-Remediation of Polluted Anaerobic Stagnant Waters. *Chem. Commun.* **2016**, *52*, 5550−5553.

(9) Mou, F.; Chen, C.; Zhong, Q.; Yin, Y.; Ma, H.; Guan, J. Autonomous Motion and Temperature-Controlled Drug Delivery of Mg/Pt-Poly (N-Isopropylacrylamide) Janus Micromotors Driven by Simulated Body Fluid and Blood Plasma. *ACS Appl. Mater. Interfaces* **2014**, *6*, 9897−9903.

(10) Howse, J. R.; Jones, R. A. L.; Ryan, A. J.; Gough, T.; Vafabakhsh, R.; Golestanian, R. Self-Motile Colloidal Particles: From Directed Propulsion to Random Walk. *Phys. Rev. Lett.* **2007**, *99*, 048102.

(11) Anderson, J. L. Colloid Transport by Interfacial Forces. *Annu. Rev. Fluid Mech.* **1989**, *21*, 61−99.

(12) Moran, J. L.; Posner, J. D.; Wheat, P. M. Locomotion of Electrocatalytic Nanomotors Due to Reaction Induced Charge Autoelectrophoresis. *Phys. Rev. E* **2010**, *81*, 065302.

(13) Solovev, A. A.; Mei, Y. F.; Urena, E. B.; Huang, G. S.; Schmidt, O. G. Catalytic Microtubular Jet Engines Self-Propelled by Accumulated Gas Bubbles. *Small* **2009**, *5*, 1688−1692.

(14) Gao, W.; Uygun, A.; Wang, J. Hydrogen-Bubble-Propelled Zinc-Based Microrockets in Strongly Acidic Media. *J. Am. Chem. Soc.* **2012**, *134*, 897−900.

(15) Manjare, M. T.; Yang, F.; Qiao, R.; Zhao, Y. Marangoni Flow Induced Collective Motion of Catalytic Micromotors. *J. Phys. Chem. C* **2015**, *119*, 28361−28367.

(16) Reigh, S. Y.; Kapral, R. Catalytic Dimer Nanomotors: Continuum Theory and Microscopic Dynamics. *Soft Matter* **2015**, *11*, 3149−3158.

(17) Gao, Y.; Yu, Y. Macrophage Uptake of Janus Particles Depends upon Janus Balance. *Langmuir* **2015**, *31*, 2833−2838.

(18) Brown, A.; Poon, W. Ionic Effects in Self-Propelled Pt-Coated Janus Swimmers. *Soft Matter* **2014**, *10*, 4016−4027.

(19) Moran, J. L.; Posner, J. D. Role of Solution Conductivity in Reaction Induced Charge Auto-Electrophoresis. *Phys. Fluids* **2014**, *26*, 042001.

(20) Popescu, M. N.; Dietrich, S.; Oshanin, G. Confinement Effects on Diffusiophoretic Self-Propellers. *J. Chem. Phys.* **2009**, *130*, 194702.

(21) Tao, Y. G.; Kapral, R. Swimming Upstream: Self-Propelled Nanodimer Motors in a Flow. *Soft Matter* **2010**, *6*, 756−761.

(22) Yang, M. C.; Wysocki, A.; Ripoll, M. Hydrodynamic Simulations of Self-Phoretic Microswimmers. *Soft Matter* **2014**, *10*, 6208−6218.

(23) Uspal, W.; Popescu, M. N.; Dietrich, S.; Tasinkevych, M. Self-Propulsion of a Catalytically Active Particle near a Planar Wall: From Reflection to Sliding and Hovering. *Soft Matter* **2015**, *11*, 434−438.

(24) Ibrahim, Y.; Liverpool, T. B. The Dynamics of a Self-Phoretic Janus Swimmer Near a Wall. *Europhys. Lett.* **2015**, *111*, 48008.

(25) Kreuter, C.; Siems, U.; Nielaba, P.; Leiderer, P.; Erbe, A. Transport Phenomena and Dynamics of Externally and Self-Propelled Colloids in Confined Geometry. *Eur. Phys. J.: Spec. Top.* **2013**, *222*, 2923−2939.

(26) Mozaffari, A.; Sharifi-Mood, N.; Koplik, J.; Maldarelli, C. Self-Diffusiophoretic Colloidal Propulsion Near a Solid Boundary. 2015, arXiv preprint arXiv:1505.07172 .

(27) Das, S.; Garg, A.; Campbell, A. I.; Howse, J.; Sen, A.; Velegol, D.; Golestanian, R.; Ebbens, S. J. Boundaries Can Steer Active Janus Spheres. *Nat. Commun.* **2015**, *6*, 8999.

(28) Popescu, M. N.; Tasinkevych, M.; Dietrich, S. Pulling and Pushing a Cargo with a Catalytically Active Carrier. *Europhys. Lett.* **2011**, *95*, 28004.

(29) Sharifi-Mood, N.; Mozaffari, A.; Córdova-Figueroa, U. Pair Interaction of Catalytically Active Colloids: From Assembly to Escape. 2015, arXiv preprint arXiv:1510.03000 .

(30) Michelin, S.; Lauga, E. Phoretic Self-Propulsion at Finite Péclet Numbers. *J. Fluid Mech.* **2014**, *747*, 572−604.

(31) Golestanian, R.; Liverpool, T.; Ajdari, A. Designing Phoretic Micro- and Nano-Swimmers. *New J. Phys.* **2007**, *9*, 126.

(32) Gao, W.; Pei, A.; Dong, R.; Wang, J. Catalytic Iridium-Based Janus Micromotors Powered by Ultralow Levels of Chemical Fuels. *J. Am. Chem. Soc.* **2014**, *136*, 2276−2279.

(33) Ibele, M.; Mallouk, T. E.; Sen, A. Schooling Behavior of Light-Powered Autonomous Micromotors in Water. *Angew. Chem., Int. Ed.* **2009**, *48*, 3308−3312.

(34) Golestanian, R.; Liverpool, T. B.; Ajdari, A. Propulsion of a Molecular Machine by Asymmetric Distribution of Reaction Products. *Phys. Rev. Lett.* **2005**, *94*, 220801.

(35) Yariv, E.; Michelin, S. Phoretic Self-Propulsion at Large Peclet Numbers. *J. Fluid Mech.* **2015**, *768*, R1.

(36) Comsol, A. *COMSOL Multiphysics User's Guide*; version September 2005.

(37) Hu, H. H.; Patankar, N. A.; Zhu, M. Direct Numerical Simulations of Fluid−Solid Systems Using the Arbitrary Lagrangian−Eulerian Technique. *J. Comput. Phys.* **2001**, *169*, 427−462.

(38) Qian, S.; Ai, Y. *Electrokinetic Particle Transport in Micro-/Nanofluidics: Direct Numerical Simulation Analysis*; CRC Press: 2012; Vol. *153*.

(39) Keh, H.; Anderson, J. Boundary Effects on Electrophoretic Motion of Colloidal Spheres. *J. Fluid Mech.* **1985**, *153*, 417−439.

(40) Keh, H. J.; Chiou, J. Y. Electrophoresis of a Colloidal Sphere in a Circular Cylindrical Pore. *AIChE J.* **1996**, *42*, 1397−1406.

(41) Qiao, R.; He, P. Modulation of Electroosmotic Flow by Neutral Polymers. *Langmuir* **2007**, *23*, 5810−5816.

DOI: 10.1021/acs.langmuir.6b01214
Langmuir 2016, 32, 5580−5592

(42) Happel, J.; Brenner, H. *Low Reynolds Number Hydrodynamics: With Special Applications to Particulate Media*; Springer Science & Business Media: 2012; Vol. *1*.
(43) Keh, H. J.; Chen, S. B. Electrophoresis of a Colloidal Sphere Parallel to a Dielectric Plane. *J. Fluid Mech.* **1988**, *194*, 377−390.
(44) Buttinoni, I.; Bialké, J.; Kümmel, F.; Löwen, H.; Bechinger, C.; Speck, T. Dynamical Clustering and Phase Separation in Suspensions of Self-Propelled Colloidal Particles. *Phys. Rev. Lett.* **2013**, *110*, 238301.
(45) Theurkauff, I.; Cottin-Bizonne, C.; Palacci, J.; Ybert, C.; Bocquet, L. Dynamic Clustering in Active Colloidal Suspensions with Chemical Signaling. *Phys. Rev. Lett.* **2012**, *108*, 268303.
(46) Simmchen, J.; Katuri, J.; Uspal, W. E.; Popescu, M. N.; Tasinkevych, M.; Sanchez, S. Topographical Pathways Guide Chemical Microswimmers. *Nat. Commun.* **2016**, *7*, 10598.
(47) Kline, T. R.; Paxton, W. F.; Mallouk, T. E.; Sen, A. Catalytic Nanomotors: Remote-Controlled Autonomous Movement of Striped Metallic Nanorods. *Angew. Chem.* **2005**, *117*, 754−756.
(48) Ai, Y.; Park, S.; Zhu, J.; Xuan, X.; Beskok, A.; Qian, S. DC Electrokinetic Particle Transport in an L-Shaped Microchannel. *Langmuir* **2010**, *26*, 2937−2944.
(49) Zhu, L.; Lauga, E.; Brandt, L. Low-Reynolds-Number Swimming in a Capillary Tube. *J. Fluid Mech.* **2013**, *726*, 285−311.
(50) Zottl, A.; Stark, H. Nonlinear Dynamics of a Microswimmer in Poiseuille Flow. *Phys. Rev. Lett.* **2012**, *108*, 218104.

DOI: 10.1021/acs.langmuir.6b01214
Langmuir 2016, 32, 5580−5592